Appl. Phys. A 86, 457–462 (2007)
DOI: 10.1007/s00339-006-3798-3

Applied Physics A
Materials Science & Processing

G.W. HO[1,2,✉]
A.S.W. WONG[3]

One step solution synthesis towards ultra-thin and uniform single-crystalline ZnO nanowires

[1] Engineering Science Programme, National University of Singapore, 9 Engineering Drive 1, 117576 Singapore
[2] Department of Electrical and Computer Engineering, National University of Singapore, 4 Engineering Drive, 117576 Singapore
[3] Institute of Materials Research and Engineering, 3 Research Link, 117602 Singapore

Received: 15 August 2006/Accepted: 16 November 2006
Published online: 23 December 2006 •

ABSTRACT Bundles of high-aspect-ratio single-crystalline ZnO nanowires were fabricated by a single-step mild hydrothermal condition without the use of a seeding layer, thus eliminating an annealing step. The growth yields nanowires of high aspect ratio (> 200). No significant lateral growth takes place with prolonged reaction time. The morphology and aspect ratio of the final products depend on the concentration of the precursors; a highly water-soluble tetradentate cyclic tertiary amine and zinc nitrate system. The nanowires grow along the [0001] direction and have an average width of < 10 nm and a narrow distribution of ±5 nm. Photoluminescence measurements of the ultra-thin nanowires exhibit a strong band-edge emission at room temperature. The highly crystalline sub tens of nanometer scale diameter nanowires can, in combination, be a good one-dimensional candidate to study optical and electronic properties.

PACS 81.16.Be; 81.07.Bc

1 Introduction

One-dimensional nanoscale materials have stimulated considerable interest recently because of their unique electronic, optical and mechanical properties as well as their potential application in nanodevices. Many attempts have been made to synthesize one-dimensional nanostructured materials. One of the widely synthesized materials is ZnO, which has important electronic and photonic properties. This is because ZnO has a direct band gap of 3.37 eV at room temperature with a large exciton binding energy of 60 meV [1]. The strong exciton energy can ensure an efficient exciton emission at room temperature under low excitation energy. Specifically, ZnO is of interest in many applications including electrodes for solar cells [2], transparent conductive coatings [3], gas sensors [4] and electro- and photoluminescent materials [5]. Many synthetic methodologies for one-dimensional ZnO nanostructures have been developed, including vapor-phase methods such as thermal evaporation [6], chemical vapor deposition [7] and metal–organic chemical vapor deposition [8], and aqueous methods including microemulsion techniques [9], direct growth in aqueous-alcohol solution [10] and hydrothermal growth [11]. The vapor-phase method usually employs vacuum, sophisticated equipment and elevated temperature which restrict the type of substrate used, in contrast to the low-cost and simple aqueous methods. Among the aqueous methods, the hydrothermal method has emerged as a powerful method for the fabrication of one-dimensional nanomaterials with some significant advantages, such as controllable structures and a cost-effective, low-temperature, substrate-independent and less-complicated technique.

There are various reports of hydrothermal growth of ZnO nanostructures. One of which was given by Vayssieres et al. [12–14] on the preparation of highly oriented ZnO microrods and microtubes and extended their work on decreasing the overall concentration of the reagents to reduce the diameter of the ZnO rods from 1–2 μm to 100–200 nm. Guo et al. [15] used a two-step approach, which involves a precoating step of a ZnO seed layer which is annealed at 300 °C and a subsequent solution deposition process, to produce ZnO submicron rods. Govender et al. [16] synthesized ZnO nanocolumns on gold-coated tin-oxide substrates by a low temperature solution method and observed room-temperature lasing throughout the visible spectrum. This finding indicates that ZnO arrays grown from solution are suitable for potential laser construction. Greene et al. [17] reported the wafer-scale growth of ZnO nanorods and studied the temperature-dependent photoluminescence (PL) properties. Even though the chemical approaches have been widely reported and have proved to be simple, economic and suitable for large-scale production, the structures of ZnO nanowires fabricated using chemical methods may not be as controllable as those of nanowires prepared via vapor-phase methods. For example, the diameter distribution of ZnO nanorods grown from solution is wider than that of nanorods prepared by vapor–liquid–solid and chemical vapor deposition methods. As a result, controlling the diameter distribution and aspect ratio of ZnO nanowires without the use of a high temperature annealed seeding layer is still an issue in the hydrothermal synthesis method. In this paper, we have shown that the growth of ultra-thin and narrow diameter distribution ZnO nanowires without a seeding layer is possible via a low-temperature and facile hydrothermal method. We demonstrate that one-step growth at relatively low temperature and concentration can yield a large quantity of high-aspect-ratio ZnO nanowires. The

✉ Fax: +65-6775-4710, E-mail: esphgw@nus.edu.sg

growth of these nanostructures presented herein shows that a good control of reactants and growth conditions can facilitate the growth of controllable diameter zinc oxide nanowires of strong ultraviolet (UV) emission properties.

2 Experimental

Both of the chemicals zinc nitrate hexahydrate ($Zn(NO_3)_2 \cdot 6H_2O$) and methenamine ($C_6H_{12}N_4$) were analytical-grade reagents and were used without further purification. In a typical procedure, the aqueous precursors (0.0001–0.1 M) of zinc nitrate hydrate and methenamine (1 : 1 ratio) were dissolved in deionized water. They were prestirred vigorously, which resulted in the formation of a white precipitate with visible turbidity. The precursor was then transferred into an autoclavable bottle with a tight polypropylene screw cap. The liquid precursors occupied about 60%–70% of the total volume of the bottle. Bare and properly cleaned substrates such as silicon wafers and microscope glass slides were used for the growth and were placed in the bottles before tightening the caps. The bottles were then placed in a preheated oven at a relatively low temperature of 85 °C for various reaction times. For the experiments studying the effect of concentration, the ratio of Zn–amine remained constant at 1 : 1. Subsequently, the final products were washed with distilled water and then dried at 120 °C for 60 min to remove any residual salts and organic material. The crystallography and structures of the as-synthesized nanostructures were analyzed using a transmission electron microscope (TEM, Philips FEG CM300) and

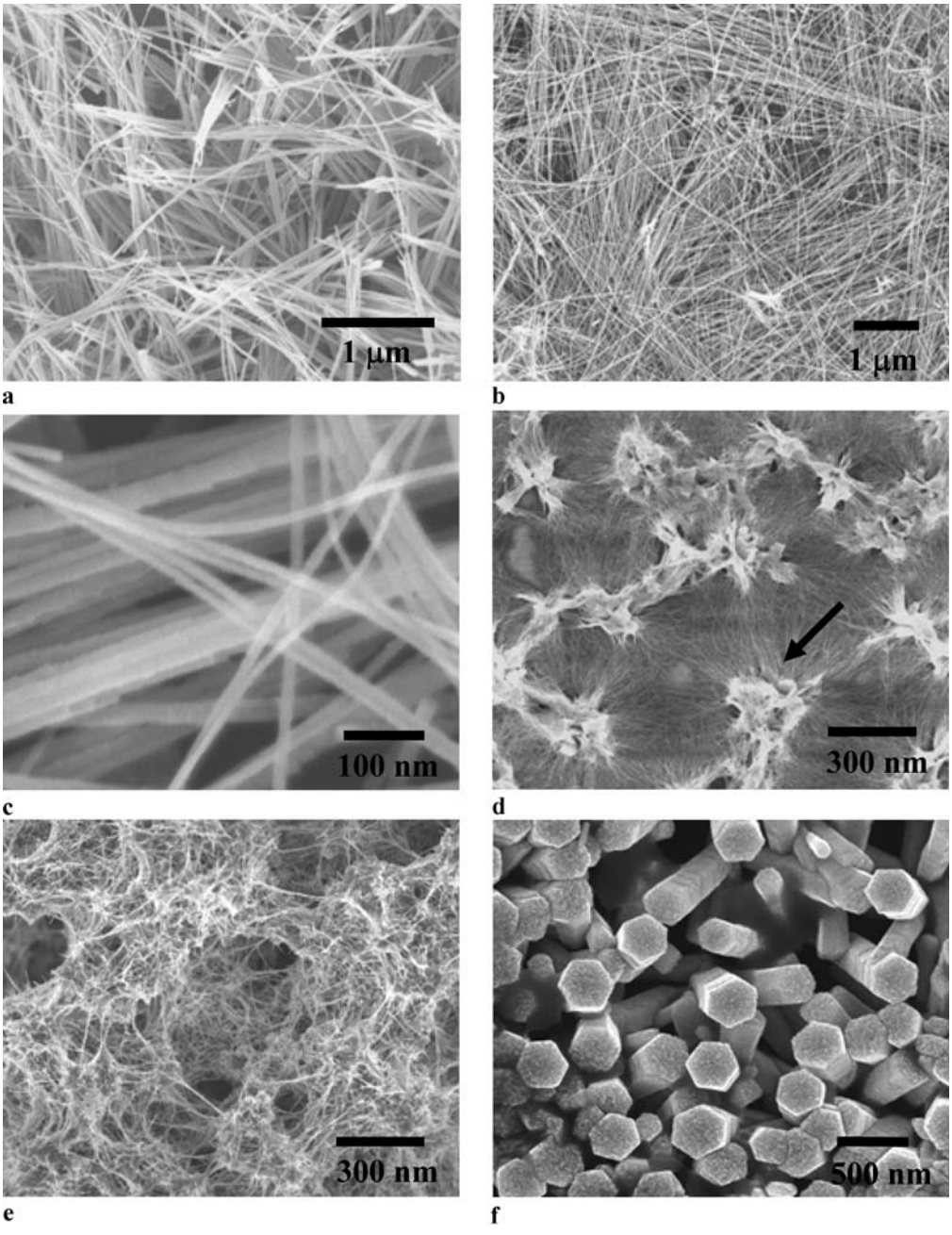

FIGURE 1 SEM images of ZnO nanostructures grown at different precursor concentration and reaction time conditions. (**a**) 0.001 M for 8 h, (**b**, **c**) 0.001 M for 24 h, (**d**) 0.0001 M for 8 h, (**e**) 0.0001 M for 24 h and (**f**) 0.1 M for 8 h

an X-ray diffractometer (XRD, Philips X-ray diffractometer equipped with a graphite monochromator, Cu K_α radiation, $\lambda = 1.541$ Å). The morphologies were characterized using a scanning electron microscope (SEM, Jeol FEG JSM 6700 F, secondary electron imaging) and PL properties were measured using an Accent RPM 2000 rapid photoluminescence mapping system with a He–Cd laser (325 nm, 1.8 mW).

3 Results and discussion

Figure 1a shows a low-resolution SEM micrograph of ZnO nanostructures grown on the substrate at a precursor concentration of 0.001 M after a 8 h hydrothermal process. The morphology shows bundles of thin nanowires vertically aligned on the substrate. The bundling of the thin and long nanowires is due to their susceptibility to the capillary force disruption of aqueous solution. Figure 1b shows the morphology after undergoing a hydrothermal process for 24 h; the bundles of ZnO nanowires grew in length and density. At high magnification (Fig. 1c), it is observed that the thin nanowires have a narrow diameter distribution of $\sim$ 20–40 nm and a length of $\sim$ 5–10 μm. In addition, Fig. 1c also reveals that the densely grown nanowires are well aligned along the non-polar facets and physically overlap each other. This indicates that the bundling of the nanowires is not a result of intergrowth or branching of a single nanorod but rather they were individually grown. Sagunan et al. [18] have reported bundling of ZnO nanowires, however with a lower aspect ratio, randomly aligned and less densely grown, which were prepared by a two-step synthesis method based on seeding layers. It is worthwhile emphasizing that our synthesis method requires no seeding layer and no significant lateral growth was observed even after an extended growth of 30 h. By further decreasing the precursor concentration to 0.0001 M under a controlled reaction time of 8 h, the diameters of the ZnO nanowires can be further reduced to 4–10 nm while the morphology transformed into a cobweb-like structure (Fig. 1d). It is noted that the growth morphology looks different from that presented in Fig. 1a. In this case there is more obvious bundling of the nanowires along with the presence of irregularly shaped crystals as indicated by an arrow in Fig. 1d. The ultra-thin nanowires were observed to nucleate and grow mainly around the aggregated irregularly shaped crystals. Similarly, over an extended time of 24 h, the density and length of the nanowires increased (Fig. 1e). When the precursor is greatly increased in concentration to 0.1 M, large-diameter nanowires are obtained (Fig. 1f). These densely grown nanowires are vertically aligned on the substrate and are $\sim$ 160–560 nm in diameter and $\sim$ 3–5 μm in length. All the as-synthesized structures were identified to be ZnO using SEM energy-dispersive X-ray spectroscopy (EDX) with a detection limit of < 1 at. %. In addition, we observed that the diameter distribution (Fig. 2) becomes narrower with the decrease of precursor concentration based on SEM micrographs covering an area of 10×10 μm^2. One has to take into account that the values obtained should be treated as an estimation, mostly to illustrate the relative values. For nanowires grown

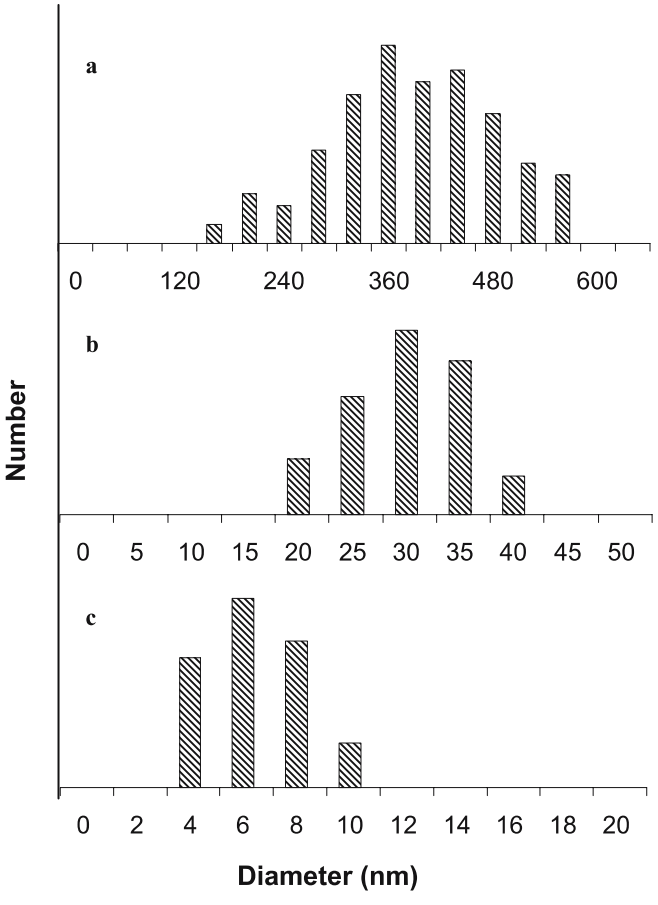

FIGURE 2 Diameter distributions of ZnO nanowires grown at precursor concentrations of (**a**) 0.1 M, (**b**) 0.001 M and (**c**) 0.0001 M

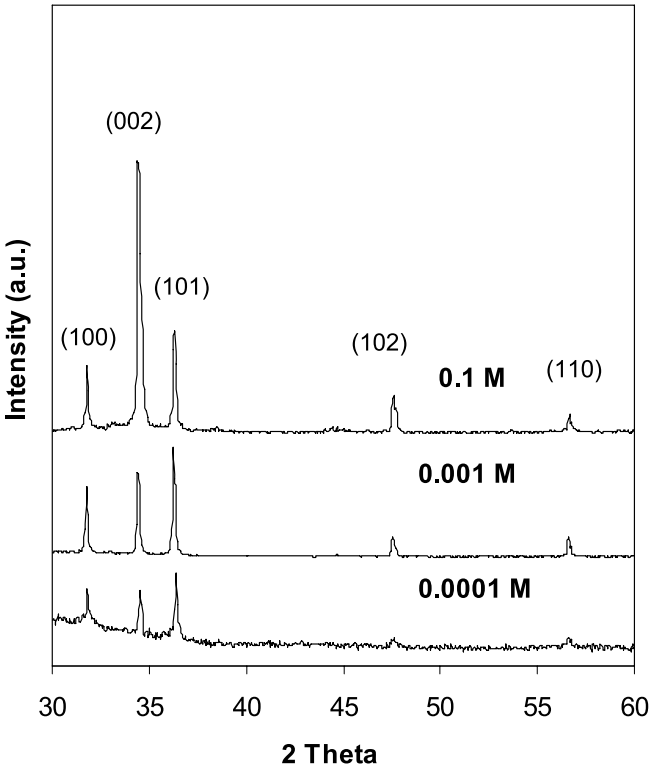

FIGURE 3 XRD patterns of ZnO nanostructures obtained from various precursor concentrations

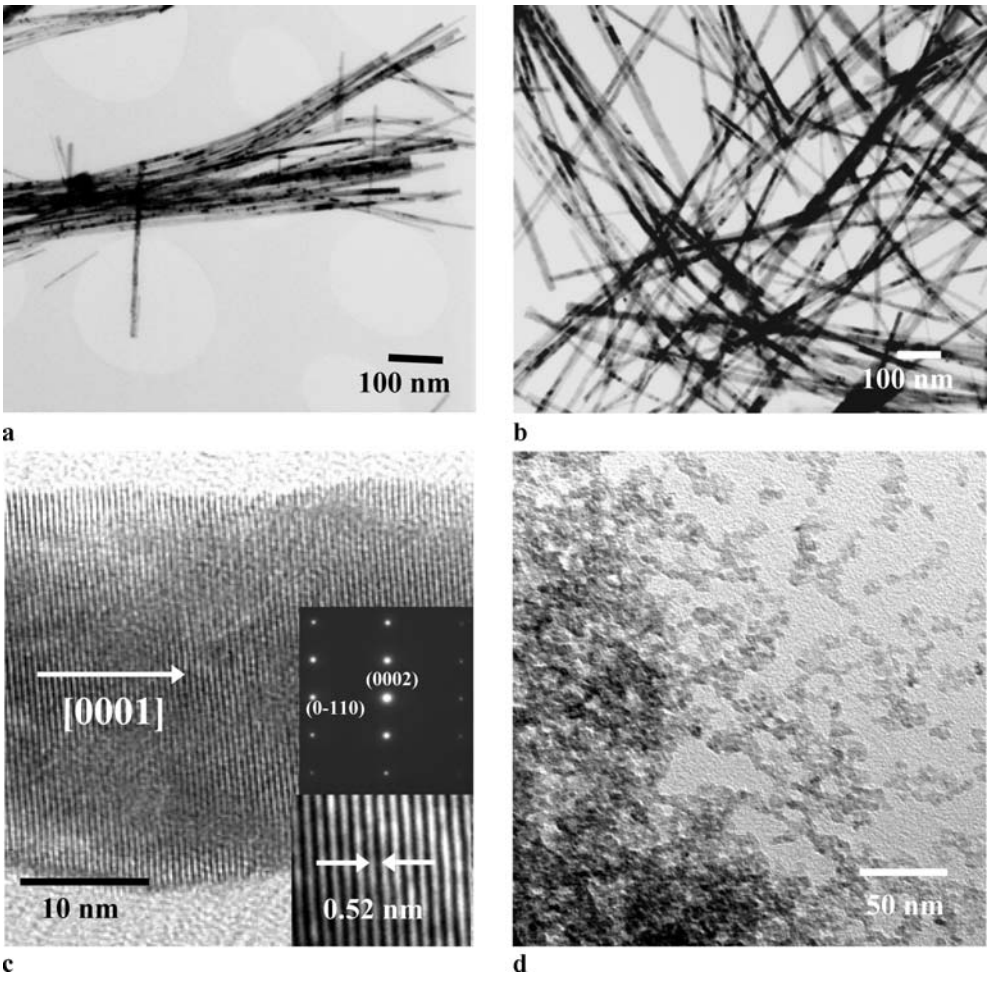

FIGURE 4 TEM images of ZnO nanostructures dispersed on holey carbon grid. (**a**, **b**) Bright-field, low-magnification images of bundles and dispersed nanowires. (**c**) High-resolution image of an individual nanowire; the *insets* show corresponding selected area diffraction patterns and high-resolution lattice fringes with calculated and measured interplanar distance of ~ 0.52 nm. (**d**) Agglomerated ZnO nanoparticles recovered from the reactive solution

in 0.1 M precursor solution, the diameter distribution has a 400 nm range width and, as the precursor concentration is reduced to 0.001 M and 0.0001 M, the distribution of the diameter is reduced to 20 nm and 8 nm range width, respectively. This indicates that thin and uniform-diameter nanowires can be synthesized at low concentration where low supersaturation is believed to be responsible for the small diameter and narrow size distribution of the ZnO nanowires.

To confirm the phase composition and crystallinity of the synthesized nanostructures, we have conducted XRD pattern analyses. Figure 3 shows the XRD pattern of the sample prepared by a hydrothermal process at various precursor concentrations. All the diffraction peaks can be indexed as the hexagonal wurtzite ZnO structure (space group ($P6_3mc$) with the lattice constants $a = 3.249$ Å and $c = 5.206$ Å, which is consistent with the values in the standard card JCPDS 36-1451 [15]. The diffraction patterns indicate pure and good-crystallinity ZnO nanostructures with the absence of other minerals. It is also noted that all the XRD patterns look similar except for the intensities of the peaks, which increase with the concentration of the precursor. The relative higher diffraction intensity as measured from the 0.1 M concentration may indicate that ZnO nanostructures grown at increased concentration have improved crystallinity in addition to a better orientation with respect to the substrate [15]. Structural analyses using TEM were also carried out on ZnO nanostructures grown at 0.001 M. Figure 4a shows the low-magnification image of a bundle of nanowires dispersed on a TEM grid. We do not observe any branching structures; notionally, one would expect each aggregate of ZnO crystallites to have developed into an individual nanowire. During the preparation for the TEM studies, some of the bundles of nanowires were separated (Fig. 4b), which further proves that the nanowires were individually grown rather than branched or intergrown from a single structure. To further obtain structural information of the nanowires, a high-resolution TEM image was obtained (Fig. 4c). The corresponding diffraction pattern and the lattice-plane spacing (approximately 0.52 nm) (Fig. 4c, insets) can be identified to be hexagonal ZnO structure [19]. In addition, this indicates that the ZnO nanowires have preferentially grown along the [0001] direction [20]. TEM EDX analyses (not presented here) were carried out on various positions along the nanowires to confirm their chemical composition to be pure ZnO, which proves to be consistent with the SEM EDX and XRD results.

To understand the growth mechanism, it is necessary to know the general chemical reaction process as well as the growth habits of the zinc oxide crystals. In a typical aqueous solution, metal cations M^{x+} are solvated by water giving rise to aquo ions, typically $[M(OH_2)_n]^{x+}$. The $M-OH_2$ bond is polarized to promote deprotonation of the coordinated water. In dilute solutions, a range of monomeric species and/or other

hydroxyl species [$M(OH)_n$] may be formed [20]. In order to form the polynuclear species, which then develop into metal oxide, reactions involving dehydration must occur [21]. At a reaction temperature of 85 °C, the Zn–amine complex decomposed and released Zn^{2+} ions. The cations then formed $Zn(OH)_2$ and ZnO under the hydrothermal process as shown in (1).

$$Zn^{2+} + 2OH^- \rightarrow Zn(OH)_2 \rightarrow ZnO + H_2O \quad (1)$$

With regard to crystal habits, a typical wurtzite ZnO crystal has polar faces ((0001) basal plane) and non-polar faces ($(11\bar{2}0)$ and $(10\bar{1}0)$ planes). Polar faces with surface dipoles are thermodynamically less stable than non-polar faces, which tend to rearrange themselves to minimize surface energy [19]. As a result, the growth along the [0001] direction has a faster growth rate than that along other directions. In addition, our aqueous growth employed the non-polar chelating ligand methenamine to preferentially attach to the non-polar facets of the ZnO nanostructures and exposed the (0001) plane for growth, thus further enhancing one-dimensional growth [22]. It is important that the methenamine is allowed to react with the Zn nitrate through vigorous prestirring before exposing at a relatively low temperature of 85 °C to achieve slow decomposition of the Zn–amine complex. Careful examination using TEM of the material precipitated from the reactive solution in parallel with the growth reveals ZnO crystallites with an average diameter of 3–5 nm as shown in Fig. 4d. The agglomeration of the nuclei (ZnO crystallites) was preformed in the solution by homogeneous reaction. The early precipitation whereby solid nuclei formed as the liquid precursors are thermodynamically unstable, in supersaturated condition. The growth of the ZnO nanostructures points to a complex series or parallel chemical reaction of crystallites cluster-by-cluster agglomeration in the solution which, in combination or subsequently, leads to the absorption at the substrate surface. At low precursor concentration, the ZnO crystallites formed ultra-thin nanowires and irregularly shaped crystals with multiple interfaces. Due to higher surface energy at the interfaces, reactive species will adsorb on the interfaces, resulting in a decrease of surface energy and generation of active sites [22]. The active sites will trigger the nucleation at the interface promoting the formation of nanowires radiating outwards to form cobweb-like structures. Conceivably, the existence of the agglomerated crystals may have affected the interplay between the Zn^{2+} ion release pattern and the attendant hydrodynamics at nanoscale such that the localized regions around them have a relatively high concentration of ZnO complex nucleates. As the concentration of the precursor is increased slightly, the ZnO crystallites form bundles of well-aligned instead of randomly aligned nanowire nucleates. At even higher precursor concentration, only thick vertically aligned nanowires are synthesized, as one would expect that the supersaturation to be high and growth of closely packed nanorods are promoted.

The UV and visible PL of the ZnO nanostructures were measured using a 325-nm He–Cd laser at room temperature. All the samples showed a band-edge emission around 380 nm and a broad peak located between 430 and 840 nm,

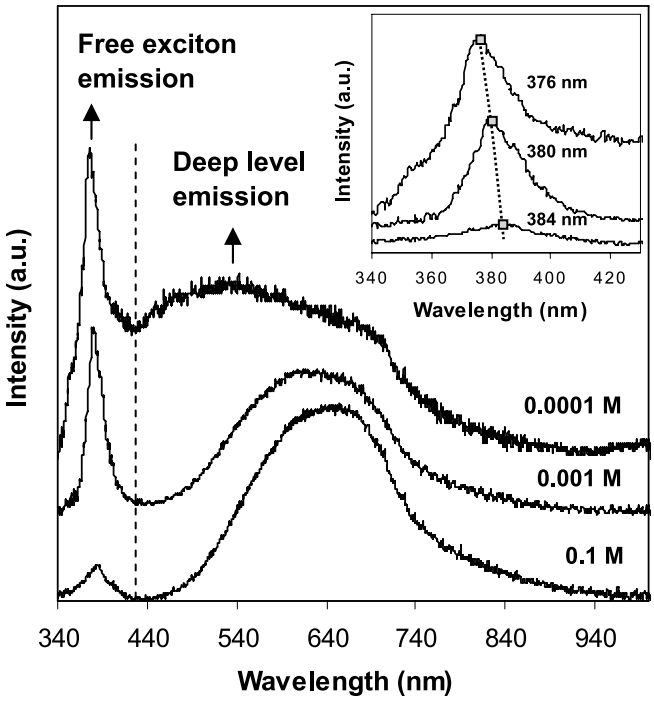

FIGURE 5 Room-temperature PL spectra of ZnO nanowires at different precursor concentrations. The *inset* shows the magnified band-edge emission with a 70-meV spectral shift with decreasing diameter

which can be attributed to free-exciton annihilation and deep-level emission, respectively (Fig. 5) [17, 23, 24]. The narrow UV and broad visible peaks are familiar in the PL spectrum of ZnO nanostructures or ZnO single-crystalline films. As the concentration of the precursor or rather the diameters of the ZnO nanowires decreased, it is observed that broadening of visible emission bands and peak shifting of the band-edge emission occur. The ultra-thin nanowires (0.0001 M) exhibit a near-band-edge emission at 376 nm (3.30 eV) as compared to the thick nanowires (0.1 M), which has their peak at 384 nm (3.23 eV). The shift of the band-edge emission is approximately 75 meV as shown in the inset of Fig. 5. It is known that a measured room-temperature PL spectrum consists of a superimposed free-exciton peak and its phonon replicas [25, 26]. The relative intensity of the dominating emission is determined by crystallinity quality, which can lead to a spectral shift up to 80 meV [25]. In addition, a spectral shift from 387 nm (3.20 eV) to 373 nm (3.32 eV) has also been reported by Wang et al. in the PL properties of ultra-thin (6-nm width) and thick (200-nm width) ZnO nanobelts [27]. They addressed the crystallinity quality of the thicker nanobelt, which exhibits less intrinsic defects (mainly stacking faults) and the highly defective ultra-thin nanobelt, which consists of stacking faults, edge dislocations and atomic plane distortion defects [27]. In view of this, the spectral shift of the nanowires with decreasing diameter is attributed to an increase in crystal defects and not the confinement effect, which is likely to be observed at low temperature [28]. It has been suggested that interstitial zinc may cause red and infrared (IR) emission [29], while singly ionized oxygen vacancies may result in green emission [19]. Here, we see that the optical properties of ZnO nanowires are sensitive to the size and structure; however, more investigations are needed to definitively iden-

tify the types of defects that are responsible for the observed emissions.

4 Conclusions

In summary, we have realized a high-yield synthesis of ultra-thin (< 10 nm) ZnO nanostructures via a low-temperature and mild hydrothermal reaction. We have reasoned that through the control of nucleation events by an organic additive and modification of the amount of Zn concentration we can facilitate the growth of high-aspect-ratio (> 200) nanowires. Thus, attempts to improve the aspect ratio and diameter uniformity were proved to be successful. The as-synthesized ZnO nanostructures exhibit hexagonal wurtzite structure, high crystallinity, uniform distribution and strong UV emission. In short, this paper provides a simple solution route eliminating preparation and annealing of a seeding layer step to obtain a controllable diameter of ZnO nanostructures, which are expected to be useful for the production of other similar oxide-based nanomaterials. Other external factors such as reaction pressure, ionic strength, surfactant and solvent are in the process of being studied and are also found to influence the morphology and alignment of ZnO nanostructures.

REFERENCES

1 M. Zamfirescu, A. Kavokin, B. Gil, G. Malpuech, M. Kaliteevski, Phys. Rev. B **65**, 161 205 (2002)
2 M. Law, L. Greene, J.C. Johnson, R. Saykally, P. Yang, Nat. Mater. **4**, 455 (2005)
3 T. Minami, J. Vac. Sci. Technol. A **17**, 1765 (1999)
4 Q. Wan, Q.H. Li, Y.J. Chen, T.H. Wang, X.L. He, J.P. Li, C.L. Lin, Appl. Phys. Lett. **84**, 3654 (2004)
5 C.M. Mo, Y.H. Li, Y.S. Lin, Y. Zhang, L.P. Zhang, J. Appl. Phys. **83**, 4389 (1998)
6 P.X. Gao, Z.L. Wang, Small **1**, 945 (2005)
7 J.J. Wu, S.C. Liu, Adv. Mater. **14**, 215 (2002)
8 B.P. Zhang, N.T. Binh, Y. Segawa, K. Wakatsuki, N. Usami, Appl. Phys. Lett. **83**, 1635 (2003)
9 J. Zhang, L. Sun, H. Pan, C. Liao, C. Yan, New J. Chem. **26**, 33 (2002)
10 B. Cheng, W. Shi, J.M. Russell-Tanner, L. Zhang, E.T. Samulski, Inorg. Chem. **45**, 1208 (2006)
11 C. Pacholski, A. Kornowski, H. Weller, Angew. Chem. Int. Edit. **41**, 1188 (2002)
12 L. Vayssieres, K. Keis, S.E. Lindquist, A. Hagfeldt, J. Phys. Chem. B **105**, 3350 (2001)
13 L. Vayssieres, K. Keis, A. Hagfeldt, S.E. Lindquist, Chem. Mater. **13**, 4395 (2001)
14 L. Vayssieres, Adv. Mater. **15**, 464 (2003)
15 M. Guo, P. Diao, S. Cai, J. Solid State Chem. **178**, 1864 (2005)
16 K. Govender, D.S. Boyle, P. O'Brien, D. Brinks, D. West, D. Coleman, Adv. Mater. **14**, 1221 (2002)
17 L.E. Greene, M. Law, J. Goldberger, F. Kim, J.C. Johnson, Y. Zhang, R.J. Saykally, P. Yang, Angew. Chem. Int. Edit. **42**, 3131 (2003)
18 A. Sagunan, H.C. Warad, M. Boman, J. Dutta, J. Sol-Gel Sci. Technol. **39**, 49 (2006)
19 D. Wang, C. Song, J. Phys. Chem. B **109**, 12 697 (2005)
20 K. Govender, D.S. Boyle, P.B. Kenway, P. O'Brien, J. Mater. Chem. **14**, 2575 (2004)
21 W.J. Li, E.W. Shi, W.G. Zhong, Z.W. Yin, J. Cryst. Growth **203**, 186 (1999)
22 X. Gao, X. Li, W. Yu, J. Phys. Chem. B **109**, 1155 (2005)
23 H.S. Qian, S.H. Yu, J.Y. Gong, L.B. Luo, L.L. Wen, Cryst. Growth Des. **5**, 935 (2005)
24 Y.R. Lin, S.S. Yang, S.Y. Tsai, H.C. Hsu, S.T. Wu, I.C. Chen, Cryst. Growth Des. **6**, 1951 (2006)
25 D.A. Lucca, D.W. Hamby, M.J. Klopfstein, G. Cantwell, Phys. Stat. Solidi B **229**, 845 (2002)
26 W. Shan, W. Walukiewicz, J.W. Ager III, K.M. Yu, H.B. Yuan, H.P. Xin, G. Cantwell, J.J. Song, Appl. Phys. Lett. **86**, 191 911 (2005)
27 X. Wang, Y. Ding, C.J. Summers, Z.L. Wang, J. Phys. Chem. B **108**, 8773 (2004)
28 M. Koyano, P. Quocbao, L.T. Thanhbinh, L. Hongha, N. Ngoclong, S. Katayama, Phys. Stat. Solidi A **193**, 125 (2002)
29 M. Gomi, N. Oohira, K. Ozaki, M. Koyano, Japan. J. Appl. Phys. **42**, 481 (2003)